The Meteoritical Society

Meteoritics & Planetary Science 49, Nr 2, 215–227 (2014)
doi: 10.1111/maps.12247

Mineral chemistry of MUSES-C Regio inferred from analysis of dust particles collected from the first- and second-touchdown sites on asteroid Itokawa

Tomoki NAKAMURA[1*], Aiko NAKATO[1], Hatsumi ISHIDA[1], Shigeru WAKITA[1], Takaaki NOGUCHI[2], Michael E. ZOLENSKY[3], Masahiko TANAKA[4], Makoto KIMURA[2], Akira TSHUCHIYAMA[5], Toshihiro OGAMI[1], Takahito HASHIMOTO[6], Mitsuru KONNO[6], Masayuki UESUGI[7], Toru YADA[7], Kei SHIRAI[7], Akio FUJIMURA[7], Ryuji OKAZAKI[8], Scott. A. SANDFORD[9], Yukihiro ISHIBASHI[7], Masanao ABE[7], Tatsuaki OKADA[7], Munetaka UENO[7], and Junichiro KAWAGUCHI[7]

[1]Division of Earth and Planetary Materials Science, Laboratory for Early Solar System Evolution, Graduate School of Science, Tohoku University, Aoba, Sendai, Miyagi 980-8578, Japan
[2]College of Science, Ibaraki University, 2-1-1 Bunkyo, Mito, Ibaraki 310-8512, Japan
[3]ARES, NASA Johnson Space Center, Houston, Texas 77058, USA
[4]WEBRAM, SPring-8, National Institute for Materials Science, Sayo, Hyogo 679-5198, Japan
[5]Department of Earth and Space Science, Graduate School of Science, Osaka University, Toyonaka 560-0043, Japan
[6]Hitachi High-Technologies Corporation, 882 Ichige, Hitachinaka, Ibaraki 312-8504, Japan
[7]JAXA-ISAS, 3-1-1 Yoshinodai, Sagamihara, Kanagawa 229-8510, Japan
[8]Department of Earth and Planetary Science, Faculty of Science, Kyushu University, Hakozaki, Fukuoka 812-8581, Japan
[9]NASA Ames Research Center, Moffett Field, California, USA
[*]Corresponding author. E-mail: tomoki@m.tohoku.ac.jp

(Received 14 October 2013; revision accepted 30 October 2013)

Abstract–The mineralogy and mineral chemistry of Itokawa dust particles captured during the first and second touchdowns on the MUSES-C Regio were characterized by synchrotron-radiation X-ray diffraction and field-emission electron microprobe analysis. Olivine and low- and high-Ca pyroxene, plagioclase, and merrillite compositions of the first-touchdown particles are similar to those of the second-touchdown particles. The two touchdown sites are separated by approximately 100 meters and therefore the similarity suggests that MUSES-C Regio is covered with dust particles of uniform mineral chemistry of LL chondrites. Quantitative compositional properties of 48 dust particles, including both first- and second-touchdown samples, indicate that dust particles of MUSES-C Regio have experienced prolonged thermal metamorphism, but they are not fully equilibrated in terms of chemical composition. This suggests that MUSES-C particles were heated in a single asteroid at different temperatures. During slow cooling from a peak temperature of approximately 800 °C, chemical compositions of plagioclase and K-feldspar seem to have been modified: Ab and Or contents changed during cooling, but An did not. This compositional modification is reproduced by a numerical simulation that modeled the cooling process of a 50 km sized Itokawa parent asteroid. After cooling, some particles have been heavily impacted and heated, which resulted in heterogeneous distributions of Na and K within plagioclase crystals. Impact-induced chemical modification of plagioclase was verified by a comparison to a shock vein in the Kilabo LL6 ordinary chondrite where Na-K distributions of plagioclase have been disturbed.

INTRODUCTION

The Hayabusa spacecraft succeeded in recovering thousands of particles from a smooth terrain, called MUSES-C Regio, of the near-Earth S-type asteroid Itokawa (e.g., Binzel et al. 2001; Abe et al. 2006). Hayabusa landed on the asteroid twice (Yano et al. 2006). During the first touchdown, the spacecraft appears

to have drifted toward the southern pole region after it received an obstacle warning measurement and then Hayabusa bounced twice at a slow speed, followed by the unplanned 30 min residence on MUSES-C Regio (Kawaguchi et al. 2006). Therefore, Hayabusa sampled particles from the southern parts of the smooth terrain upon this first touchdown. During the second touchdown, the Hayabusa sampling horn touched at the approximate center of the Regio terrain (Yano et al. 2006). Therefore, the Hayabusa spacecraft collected particles of MUSES-C Regio at two different sites approximately 100 m apart. In the present study, we focus on the comparison of the mineral chemistry between particles recovered from the two touchdown sites.

The particles collected during the first touchdown were stored in room B in the sample catcher device in the sample recovery capsule, while those collected at the second touchdown were deposited in room A (Nakamura et al. 2011; Yada et al. 2012). The sample catcher has a cylindrical shape and the upper part of the cylinder is room A, while the lower part is room B (see Figs. S2 and S4A in Nakamura et al. 2011). The two rooms are separated by an aluminum plate, but there is a thin clearance gap (>0.3 mm) between the aluminum plate and the wall of the cylinder (Fig. S4A in Nakamura et al. 2011), and thus small particles can move back and forth between room A and B. In addition, during the sample capture process, particles went through the same trajectory from the surface of MUSES-C Regio to the sampling horn and then to the catcher. Therefore, some particles stored in room B may actually have been collected at the second touchdown and vice versa. However, in this paper, we assume that the room A and room B particles we analyzed are those collected from the second and the first touchdown sites, respectively, because particles in the two rooms seem not to have mixed (Yada et al. 2012).

Particles in rooms A and B were recovered onto round silica glass plates attached to the sample catcher, by knocking the outside of catcher 10–20 times with a stainless steel rod (Nakamura et al. 2011; Yada et al. 2012). This entire procedure was performed by Tomoki Nakamura. He knocked on room A harder than room B, because room B contained some metallic parts that faced the round silica glass and which would break the glass if they moved. The quantity of room A particles collected onto the silica plate is larger than that from room B (Yada et al. 2012). Currently, it is uncertain whether room A actually contains significantly more particles than room B or if the harder impacts are responsible for the greater number of particles from room A.

SAMPLES AND EXPERIMENTS

In the course of initial analysis, whose results are described separately in Nakamura et al. (2011) and in this paper, we analyzed 48 particles, among which 42 are from room A and 6 are from room B. During the first round of initial analysis (February to March of 2011), we analyzed 38 room A particles (Nakamura et al. 2011; Tsuchiyama et al. 2011; Yurimoto et al. 2011) and during the second round, 10 particles: 4 from room A (RA-QD02-0049-2, RA-QD02-0017, RA-QD02-0033, RA-QD02-0064) and 6 from room B (RB-QD04-0006, RB-QD04-0023, RB-QD04-0025, RB-QD04-0049, RB-QD04-0022, RB-QD04-0026). Sample handling and experimental procedures were the same during the first and second initial analysis and details are given in Nakamura et al. (2011). We first analyzed individual particles by synchrotron X-ray diffraction (S-XRD) at KEK (Nakamura et al. 2011) and at SPring-8 (Tanaka et al. 2013) and by microtomography at SPring-8 (Tsuchiyama et al. 2011). Second, we microtomed some of the particles for observation by a transmission electron microscope (TEM: Noguchi et al. 2011) and then all particles were polished to flat surfaces. Finally, we analyzed the polished surfaces by a field-emission electron microprobe equipped with both wavelength- and energy-dispersive spectrometers (FE-EPMA/WDS/EDS) and a field-emission scanning electron microscope equipped with an EDS and electron backscattered diffraction (FE-SEM/EDS/EBSD). All quantitative compositional data of minerals used in this paper were obtained from FE-EPMA/WDS analysis. Approximately 5 μm interval grid analyses were made within individual mineral crystals. FE-EPMA/WDS permits collection of compositional data from an area (approximately $1 \times 1\ \mu m^2$) that is much smaller than normal EPMA, without beam overlap to neighboring mineral phases. In addition to Itokawa particles, a polished section was prepared of the Kilabo LL6 chondrite (Russell et al. 2003) featuring a large shock vein, which was also analyzed by FE-EPMA/WDS/EDS and S-XRD to permit comparisons of mineral chemistry.

RESULTS

Individual Itokawa Particles

We have already reported the basics of the mineralogy and mineral chemistry of 38 of 42 room A particles we analyzed, including compositional signatures of major silicates and metal in 38 particles (Nakamura et al. 2011). In the present paper, we

describe the mineral chemistry of the 4 newly analyzed room A and 6 newly analyzed room B particles. After the description of the 10 new particles, we summarize the mineral chemistry of all particles analyzed in the initial analysis and compare these results with those of a shock vein and a host rock of the Kilabo LL6 chondrite.

New Room A Particles

RA-QD02-0033: This particle shows a strange appearance in that many small silicate subgrains with 5 μm or smaller diameters adhere to each other with many interstitial pores (Fig. 1a). The structure suggests that the particle formed by sintering of fine silicates at subsolidus temperature. Some of the silicate subgrains have rounded edges (Figs. 1b and 1c) and may thus have been abraded before the agglomeration, consistent with transportation. The fabric and structure of this particle are similar to those of RA-QD02-0013 (Nakamura et al. 2011). Fa# of olivines in this particle (the average and 1 sigma variation = 26.3 ± 0.4: n = 12) are lower than the average of 29 Itokawa olivine crystals found during the first-round initial analysis (Fa = 28.6 ± 1.1: Nakamura et al. 2011). On the other hand, low-Ca pyroxene ($Fs_{22.5 \pm 0.2}Wo_{1.0 \pm 0.3}$: n = 4) shows compositions slightly richer in MgO, but still within the range of an average of 15 low-Ca pyroxenes found in the first-round initial analysis ($Fs_{23.1 \pm 2.2}Wo_{1.8 \pm 1.7}$: Nakamura et al. 2011).

RA-QD02-0017: This is an angular particle with sharp edges. S-XRD indicates that this 50 μm particle consists almost entirely of well-crystalline olivine. Optical microscope observation of a potted butt shows weak undulatory extinction, suggestive of mild impact effects—shock level S2 (Stöffler et al. 1991). Electron-probe analysis of the polished surface indicates that olivine has a relatively homogeneous composition (Fa 29.3 ± 0.4: n = 7). Olivine contains 0.5 wt% MnO and Cr_2O_3 is below the detection limit (<0.03 wt%). These compositional signatures are consistent with olivines in other Itokawa dust particles (Nakamura et al. 2011). Small inclusions (approximately 3 μm) of diopside ($En_{50.9}Wo_{40.5}$) occur within the olivine.

RA-QD02-0049-2 and RA-QD02-0064: RA-QD02-0049-2 is one of four particles approximately 80 μm in diameter broken from the large approximately 200 μm particle RA-QD02-0049. A previous INAA study of RA-QD02-0049 indicated that it still retains a compositional signature of condensation of original material in the solar nebula (Ebihara et al. 2011). In this study, only XRD analysis was performed for this particle. RA-QD02-0049-2 shows sharp reflections of mainly olivine and minor plagioclase, which is characteristic of thermally metamorphosed, well-crystalline particles that are commonly observed in other Itokawa dust particles (Nakamura et al. 2011). RA-QD02-0064, with a size approximately 50 μm, consists dominantly of well-crystalline olivine, based upon S-XRD analysis. No ultramicrotomy, polishing, and electron-probe analysis were performed on either RA-QD02-0049-2 or RA-QD02-0064.

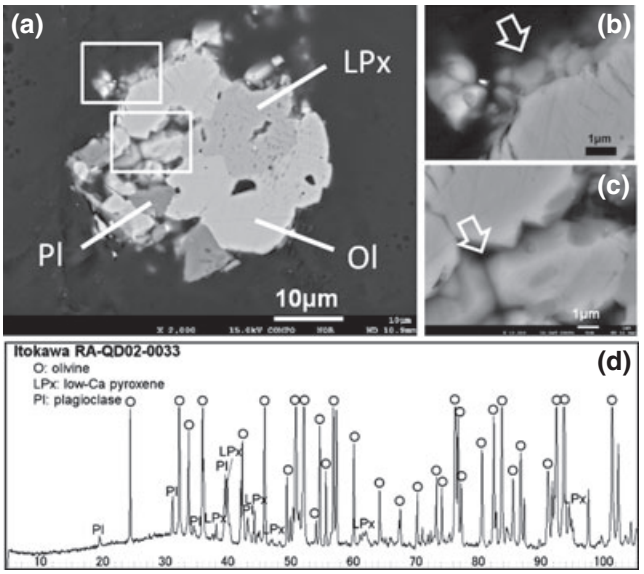

Fig. 1. Mineralogical signatures of RA-QD02-0033. a) A backscattered electron (BSE) image of a polished surface, showing small crystals of olivine (Ol), low-Ca pyroxene (LPx), and plagioclase (Pl). Triple junctions occur in the center of the particle. b, c) Enlarged views of boxed parts in (a). Surfaces of some crystals are rounded, as indicated by arrowheads. d) S-XRD pattern indicating that major phases of this particle are olivine, low-Ca pyroxene, and plagioclase. The vertical axis is X-ray intensity and the horizontal axis is diffraction angle.

Room B Particles

RB-QD04-0006: S-XRD analysis indicates that this 50 μm sized particle (Figs. 2a and 2b) consists mainly of olivine and plagioclase (Figs. 2a and 2b). Olivine is well crystalline, but plagioclase is revealed to be poorly crystalline by broad XRD reflections (Fig. 2c). BSE images of the polished surface revealed that trains of elongated pores, probably healed cracks, are present at a boundary between olivine and plagioclase and in the interior of plagioclase (Fig. 2b). A small inclusion of high-Ca pyroxene also occurs in the plagioclase. Optical microscopy indicates that olivine shows well-defined undulatory extinction suggestive of shock effects, and plagioclase is not a glass (maskelynite) consistent with S-XRD results. Electron-probe analysis of olivine and plagioclase indicates that their compositions are slightly variable within crystals: $Fa_{25.9 \pm 1.1}$ (n = 9) and $Ab_{86.2 \pm 2.0}Or_{3.8 \pm 1.6}$ (n = 3), respectively. The Fa is

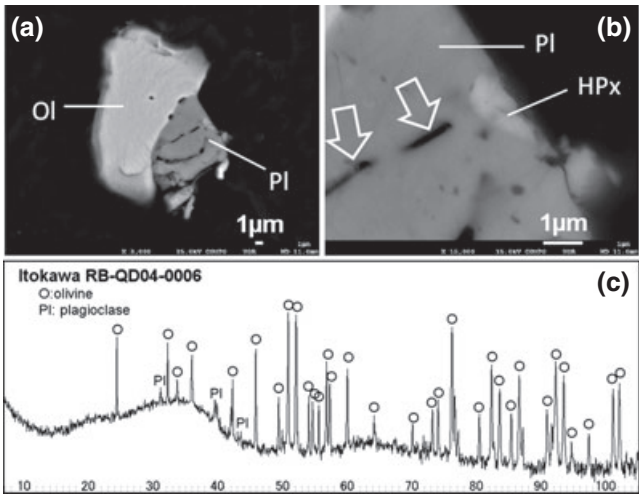

Fig. 2. Mineralogical signatures of RB-QD04-0006. a) A BSE image of a polished surface. Olivine (Ol) has a smooth surface, but plagioclase (Pl) contains many cracks. b) An enlargement of plagioclase. An inclusion of high-Ca pyroxene (HPx) is present. Some cracks appear to have been healed leaving behind a train of elongated pores, as indicated by arrowheads. c) S-XRD pattern, showing that reflections from olivine are sharp, but those from plagioclase are broad, indicating poor crystallinity. The high background around 35° comes from a glass fiber that holds the particle. The vertical axis is X-ray intensity and the horizontal axis is diffraction angle.

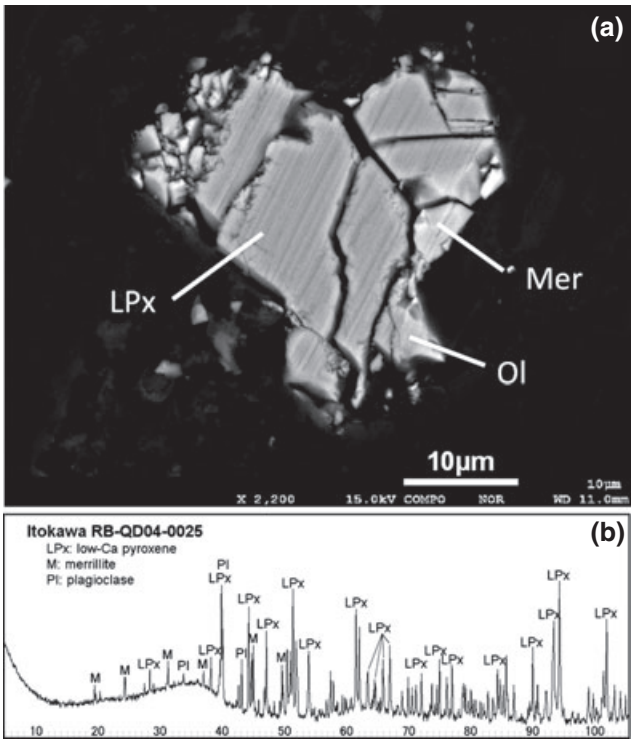

Fig. 3. Mineralogical signatures of RB-QD04-0025. a) A BSE image of a polished surface. Low-Ca pyroxene is a dominant phase and olivine and merrillite are minor phases. b) S-XRD pattern, showing that pyroxene is a major phase and merrillite and plagioclase are minor phases. Olivine appearing in (a) cannot be detected because of very low abundance (<5 vol%) and plagioclase does not appear on the polished surface in (a). The vertical axis is X-ray intensity and the horizontal axis is diffraction angle.

slightly lower and the Ab is slightly higher than the average values obtained from the first-round initial analysis ($Fa_{28.6 \pm 1.1}$ and $Ab_{83.9 \pm 1.3}$: Nakamura et al. 2011).

RB-QD04-0022: This particle is the smallest (approximately 20 μm in size) among all 49 particles described in this paper. It consists mostly of plagioclase ($Ab_{87.1 \pm 0.8}Or_{4.1 \pm 0.4}$:n = 12) with small amounts of diopside ($En_{48.3}Wo_{42.4}$: $n = 1$) according to S-XRD and FE-EPMA analyses.

RB-QD04-0025: This particle consists mainly of low-Ca pyroxene with minor amounts of plagioclase, merrillite, and olivine (Figs. 3a and 3b). Olivine was not detected by S-XRD because of very low abundance (Fig. 3b). Compositions of olivine ($Fa_{28.0 \pm 0.6}$: $n = 2$) and low-Ca pyroxene ($Fs_{23.4 \pm 1.2}Wo_{1.7 \pm 0.7}$: $n = 7$) are in the range of average Itokawa compositions, as determined previously (Nakamura et al. 2011). The composition of merrillite is similar to that in RA-QD02-0068 (Nakamura et al. 2011).

RB-QD04-0026: FE-EPMA analysis indicates that this 25 μm sized particle consists mainly of low-Ca pyroxene with a composition of $Fs_{22.8 \pm 0.5}Wo_{1.5 \pm 0.1}$: $n = 4$.

RB-QD04-0049 and RB-QD04-0023: S-XRD analysis indicates that RB-QD04-0049 consists mainly of olivine with minor plagioclase and RB-QD04-0023 is composed of olivine and high-Ca pyroxene. All silicate XRD reflections from the three particles are sharp. RB-QD04-0049 was further analyzed by INAA (Ebihara et al. forthcoming).

Compositional Properties of all Itokawa Particles

Based on the mineral chemistry of 38 particles and the existing classification schemes for chondrites (Van Schmus and Wood 1967; Huss et al. 2006), Nakamura et al. (2011) concluded that Itokawa dust particles collected in room A by the second spacecraft touchdown have mineralogies similar to LL4-6 ordinary chondrites. In this paper, among 10 new particles, 6 particles, 2 from room A (RA-QD02-0017 and RA-QD02-0033) and 4 from room B (RB-QD04-0006, RB-QD04-0022, RB-QD04-0025, and RB-QD04-0026), were analyzed by FE-EPMA for mineral chemistry. We will summarize the mineral chemistry of all 44 particles in this section.

We analyzed 5–10 points in each individual silicate crystal in all 44 particles using a single FE-EPMA with

Table 1. Averages and one sigma variations of silicates in Itokawa dust particles.

	Olivine	Low-Ca pyroxene	High-Ca pyroxene	Plagioclase
No. of particles	33	18	16	26
No. of analysis	352	163	74	163
SiO_2	37.84 ± 0.73	55.10 ± 0.85	53.82 ± 1.18	65.38 ± 1.29
TiO_2	b.d.	0.17 ± 0.06	0.37 ± 0.05	0.05 ± 0.02
Al_2O_3	0.02 ± 0.03	0.19 ± 0.09	0.66 ± 0.49	20.12 ± 0.58
FeO	25.75 ± 0.94	15.10 ± 1.32	5.52 ± 0.98	0.42 ± 0.39
MnO	0.47 ± 0.02	0.46 ± 0.03	0.24 ± 0.03	0.03 ± 0.02
MgO	36.33 ± 0.82	27.72 ± 1.01	16.57 ± 1.23	0.31 ± 0.71
CaO	b.d.	0.86 ± 0.77	20.79 ± 2.13	2.15 ± 0.14
Na_2O	0.02 ± 0.02	0.03 ± 0.03	0.57 ± 0.18	9.58 ± 0.51
K_2O	b.d.	b.d.	0.02 ± 0.04	0.92 ± 0.22
Cr_2O_3	b.d.	0.13 ± 0.10	0.72 ± 0.20	b.d.
NiO	b.d.	b.d.	b.d.	b.d.
P_2O_5	0.04 ± 0.03	b.d.	0.03 ± 0.03	0.05 ± 0.03
SO_3	b.d.	b.d.	b.d.	0.07 ± 0.10
Total wt%	100.47 ± 0.89	99.76 ± 0.89	99.31 ± 0.91	99.06 ± 1.29
Olivine (Fa#)	28.4 ± 1.2			
LPx(Fs#)		23.0 ± 2.0		
LPx(Wo#)		1.7 ± 1.5		
LPx(En#)		75.3 ± 2.3		
HPx(Fs#)			9.0 ± 1.5	
HPx(Wo#)			43.2 ± 4.3	
HPx(En#)			47.9 ± 2.9	
Pl(Or#)				5.3 ± 1.3
Pl(An#)				10.4 ± 0.8
Pl(Ab#)				84.3 ± 1.6

b.d. = below detection limits (in wt%) 0.02 for Al_2O_3, K_2O, CaO, NaO, MgO, 0.03 for SiO_2, MnO, SO_3 P_2O_5,Cr_2O_3, MnO, FeO, 0.04 for TiO_2, NiO.

the same analytical conditions. Among 44 particles, 33 olivine, 18 low-Ca pyroxene, 16 high-Ca pyroxene, and 26 plagioclase crystals were found and their average compositions and one sigma variations are given in Table 1. The mean Fa and one sigma variation of 352 analyses for 33 olivines is Fa = 28.4 ± 1.2 and the Fa distribution of the 352 analyses is shown in Fig. 4. The Fa distribution of olivine in the room B particles is within the range of that of the room A particles. One sigma variations of Fa in each olivine crystal decrease with increasing of Fa number (Fig. 5a). Both low- and high-Ca pyroxenes are found within the room B particles and their chemical compositions are almost identical to those in the room A particles. Many particles contain both olivine and low-Ca pyroxene and Fa and Fs of these particles are positively correlated (Fig. 5b).

Room B plagioclase has compositions that fall within the compositional range of room A plagioclase (Fig. 6a). Analyses of 26 plagioclase crystals indicate that Ab and Or contents show a correlation (Fig. 7a). K-feldspar (sanidine) occurs only in particle RA-QD02-0013 as exsolution lamellae in plagioclase (Fig. 6a)

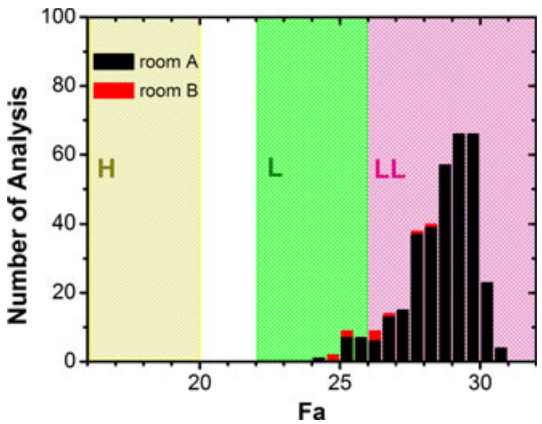

Fig. 4. Fa distribution of 352 analyses in 42 Itokawa samples, 40 from room A and 2 from room B. Average composition and one sigma variation are shown in Table 1.

(Nakamura et al. 2011). Minor minerals found in the room A particles are chromite, troilite, taenite, kamacite, apatite, and merrillite (Nakamura et al. 2011). Merrillite and apatite usually occur as small crystals up to 5 μm. Merrillite occurs in one room B particle

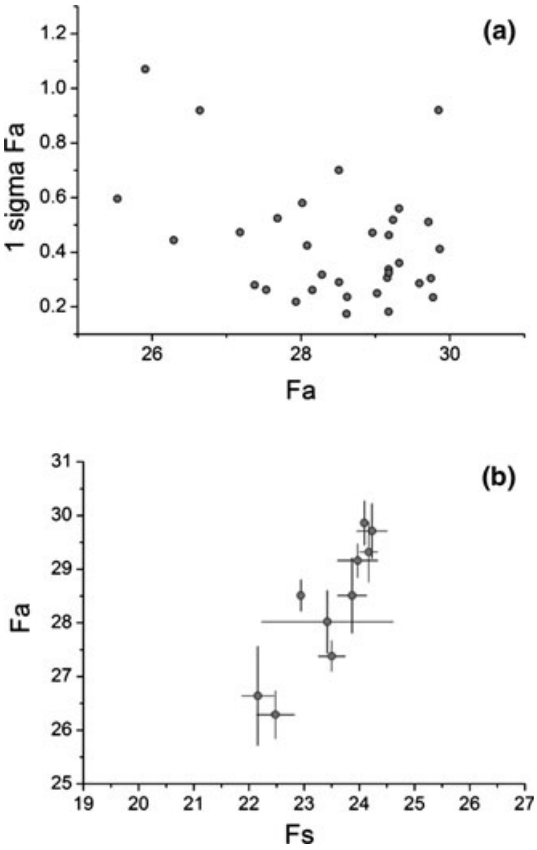

Fig. 5. a) One sigma variations of Fa in unit of Fa mol% as a function of Fa. b) Relationship between Fa and Fs of low-Ca pyroxene in 10 Itokawa particles that contain both olivine and low-Ca pyroxene. Error bars represent one sigma variations.

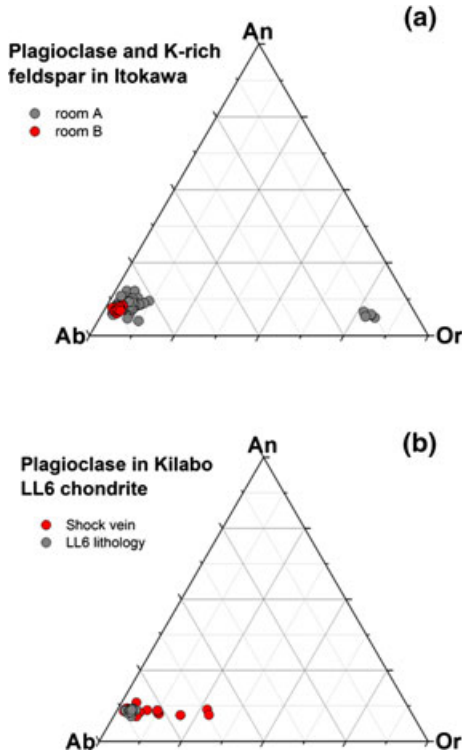

Fig. 6. a) Plagioclase compositions from 163 analyses of 26 Itokawa samples, 24 from room A and 2 from room B. Average composition and one sigma variation are shown in Table 1. b) Plagioclase compositions of the Kilabo LL6 chondrite from 41 analyses, 21 from a shock vein and 20 from the host LL6 lithology. Average composition and one sigma variation are shown in Table 3.

(Fig. 3a) and its composition is similar to that found in the room A particles (Nakamura et al. 2011). No additional minor minerals have been found from the room B particles that we analyzed.

The bulk chemical composition of 50 Itokawa particles was determined (Table 2), among which 44 were investigated in this study and by Nakamura et al. (2011) for mineral chemistry and the remaining 6 particles are analyzed and reported by Tsuchiyama et al. (2013). For calculations, we used the relative mineral abundance in each particle as determined by microtomography analysis (Tsuchiyama et al. 2013), the average chemical composition of minerals (Table 1 and Nakamura et al. [2011] for minor minerals), and the density of minerals that were obtained from the average chemical compositions (Tsuchiyama et al. 2013). The result indicates that the bulk compositional data obtained from these 50 particles are similar to those from 38 previously described Itokawa particles (Nakamura et al. 2011), all of which indicate that Itokawa dust particles from MUSES-C Regio are most similar to LL chondrites (Table 2).

However, the Itokawa dust seems to be depleted in Fe, Ni, and S and enriched in MgO and FeO compared with LL chondrites (Table 2). This can be ascribed to differences in relative mineral abundance between Itokawa and LL chondrites: troilite and FeNi metal are depleted in Itokawa (2.07 and 0.23 vol%, respectively: Tsuchiyama et al. 2013) relative to LL chondrites (5 and 2 vol%, respectively: Dunn et al. 2010). The enrichment of MgO and FeO probably results from an apparent increase of olivine and low-Ca pyroxene abundance, which is actually due to depletion of troilite and FeNi metal, because olivine/low-Ca pyroxene abundance ratios are similar between Itokawa (3.5 from Tsuchiyama et al. 2013) and LL chondrites (3.6 from Dunn et al. 2010).

The low sulfide abundance is also detected from S-type asteroid Eros and the space weathering involving the volatilization of sulfur was suggested as one of possible mechanisms that lowered the sulfide abundance (Nittler et al. 2001). Ten million years of exposure to solar cosmic rays might have removed all sulfur from the upper 5 cm of Eros (Nittler et al. 2001). In the case

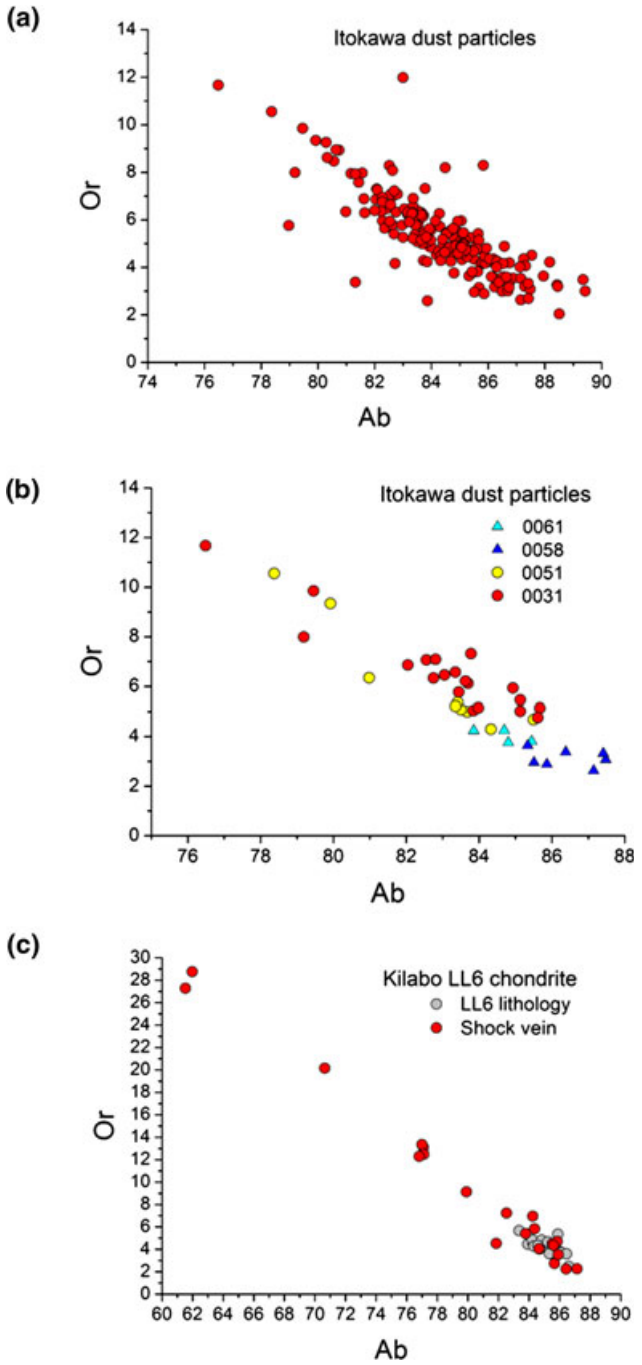

Fig. 7. Relationships between Or and Ab contents of plagioclase. a) All Itokawa particles (163 analyses). b) Selected four Itokawa particles, RA-QD02-0061, -0058, -0051, and 0031. Ab and Or contents of the former two show a limited variation, while those of the latter two show a wide variation. c) A shock vein and a host LL6 lithology of the Kilabo meteorite. An and Or contents in the shock vein show a wide variation.

of Itokawa, the exposure age of MUSES-C is shorter than 10 Myr (Nagao et al. 2011), but even such a short duration of exposure might have eroded away the sulfides from the outermost surface of Itokawa from which spacecraft Hayabusa sampled dust particles.

Mineralogical and Compositional Properties of the Kilabo LL6 Chondrite

Olivine, low- and high-Ca pyroxene, and plagioclase in a polished section (approximately 200 mm^2) of the Kilabo LL6 chondrite were observed and analyzed by FE-EPMA for mineralogical comparison to Itokawa dust particles. The Kilabo sample consists of two lithologies: a typical LL6 lithology that consists mainly of coarse (up to 100 μm diameter) olivine, pyroxene, plagioclase, FeNi metal, and troilite (Fig. 8) and another, which is a shock vein approximately 200 μm wide and 5 mm in length (Fig. 9a) where olivine, pyroxene, plagioclase, and troilite with diameters up to 50 μm occur (Fig. 9b). The shock vein sharply cuts the typical LL6 lithology (Fig. 9b).

High-magnification SEM observation of the vein indicates that, during an impact, olivine, pyroxene, plagioclase, and most of the troilite and FeNi metal were not melted, and only FeS and FeNi metal located close to the boundary were melted to form Fe-Ni-S melts (Fig. 9b). This observation indicates that temperature was elevated locally at the boundary over the Fe-Ni-S eutectic temperature (approximately 988 °C) due to friction, but major parts were not heated to such a temperature. S-XRD analysis indicates that olivine, low- and high-Ca pyroxene, and plagioclase are major mineral phases and suggests that no high-pressure minerals occur in the shock vein. The smaller size of silicates and sulfides in the vein (Fig. 9b) compared with the host LL6 lithology (Fig. 8) and the discontinuous change of texture between the vein and the host suggest that the vein was formed by comminution and frictional heating during a movement of a crack plane.

FE-EPMA analysis indicates that olivine, low- and high-Ca pyroxene, and plagioclase in the typical LL6 lithology of the Kilabo meteorite have homogeneous compositions (Table 3). The coarse grain size of plagioclase and high-Ca pyroxene and homogeneous silicate compositions verify the LL6 classification of this meteorite. Two-pyroxene thermometry (Lindsley 1983) was applied to low- and high-Ca pyroxene and gives an equilibrium temperature of 880 ± 7 °C. This temperature is similar to that obtained from other LL6 chondrites (e.g., McSween and Patchen 1989; Jones 1997), but is higher than that of the average for three Itokawa particles determined using the same geothermometer (approximately 820 °C: Nakamura et al. 2011).

Fe/(Fe+Mg) ratios of olivine and low- and high-Ca pyroxene in the Kilabo shock vein are similar to those

Table 2. Bulk composition of Itokawa particles in comparison with ordinary chondrite falls.

	Itokawa particles		LL	L	H
wt%	*This study	Nakamura et al. (2011)			
SiO_2	42.38 ± 2.84	42.45	40.6	39.7	36.6
TiO_2	0.05 ± 0.01	0.05	0.1	0.1	0.1
Al_2O_3	1.77 ± 0.18	1.80	2.2	2.3	2.1
FeO	20.65 ± 1.88	20.57	17.4	14.5	10.3
MnO	0.41 ± 0.03	0.40	0.4	0.3	0.3
MgO	29.61 ± 2.56	29.53	25.2	24.7	23.3
CaO	0.90 ± 0.16	0.86	1.9	1.9	1.7
Na_2O	0.84 ± 0.09	0.85	1.0	1.0	0.9
K_2O	0.08 ± 0.02	0.08	0.1	0.1	0.1
Cr_2O_3	0.11 ± 0.02	0.11	0.5	0.5	0.5
P_2O_5	0.06 ± 0.02	0.04	0.2	0.2	0.3
Oxides	96.86	96.76	89.7	85.3	76.2
Fe	0.28 ± 0.03	0.28	2.4	7.0	16.0
Ni	0.25 ± 0.03	0.26	1.1	1.2	1.7
FeS	2.84 ± 0.23	2.97	5.8	5.8	5.4
Total	100.23	100.27	99.0	99.3	99.4

LL, L, and H chondrite data from Jarosewich (1990).
The bulk composition is determined by modal reconstruction.
*This study is the combined data set with Nakamura et al. (2011).

Table 3. Compositional signatures of Kilabo LL6 chondrite.

	LL6 lithology		Shock vein	
Olivine (Fa#)	31.1 ± 0.5	(n = 20)	30.4 ± 0.4	(n = 23)
LPx(Fs#)	25.2 ± 0.3	(n = 20)	24.9 ± 0.3	(n = 19)
LPx(Wo#)	1.7 ± 0.2		1.9 ± 0.8	
LPx(En#)	73.1 ± 0.4		73.2 ± 0.7	
HPx(Fs#)	10.4 ± 0.6	(n = 10)	10.3 ± 0.5	(n = 5)
HPx(Wo#)	44.1 ± 0.7		44.0 ± 0.3	
HPx(En#)	45.5 ± 0.2		45.7 ± 0.5	
Pl(Or#)	4.3 ± 0.7	(n = 20)	9.3 ± 7.7	(n = 21)
Pl(An#)	10.6 ± 0.7		10.5 ± 1.1	
Pl(Ab#)	85.2 ± 0.9		80.3 ± 7.5	

in the typical LL6 lithology (Table 3). On the other hand, compositions of plagioclase differ between the two lithologies: An contents are the same, but Ab and Or contents of the shock-vein plagioclase are much more variable than those of the LL6 lithology (Fig. 6b and Table 3), which suggests redistribution of Na and K during shock heating. These results clearly indicate that shock metamorphism affects Ab and Or contents of plagioclase. Alkali element redistribution in plagioclase during impacts on LL chondrites was also suggested by Chen and El Goresy (2000) and Kovach and Jones (2010). Rubin (1992) suggests that Ca distribution within plagioclase is also subject to change during heavy impacts, although this tendency is not observed in the case of either the Kilabo shock vein or the Itokawa samples.

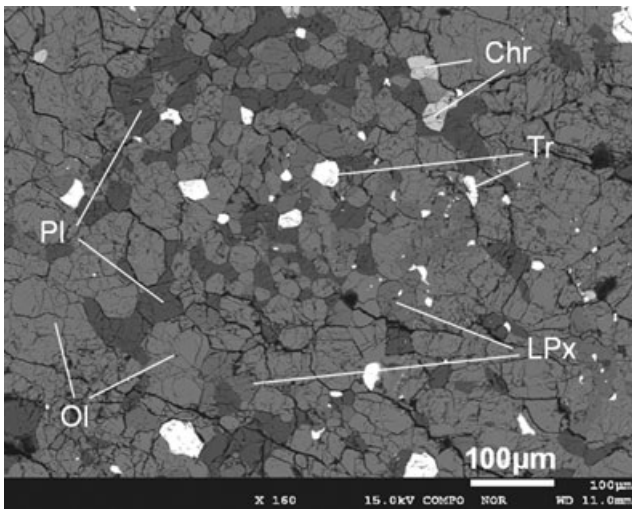

Fig. 8. A BSE image of the Kilabo LL6 chondrite. A typical LL6 lithology consisting of equigranular olivine (Ol), low-Ca pyroxene (LPx), plagioclase (Pl), chromite (Chr), and troilite (Tr).

DISCUSSION

Formation of MUSES-C Dust Particles

Itokawa dust particles in the smooth terrain, MUSES-C Regio, were mostly formed at significant depths within the parent asteroid of Itokawa by prolonged thermal metamorphism, before a large-scale impact destroyed the parent asteroid (Nakamura et al. 2011). MUSES-C Regio is considered to have formed

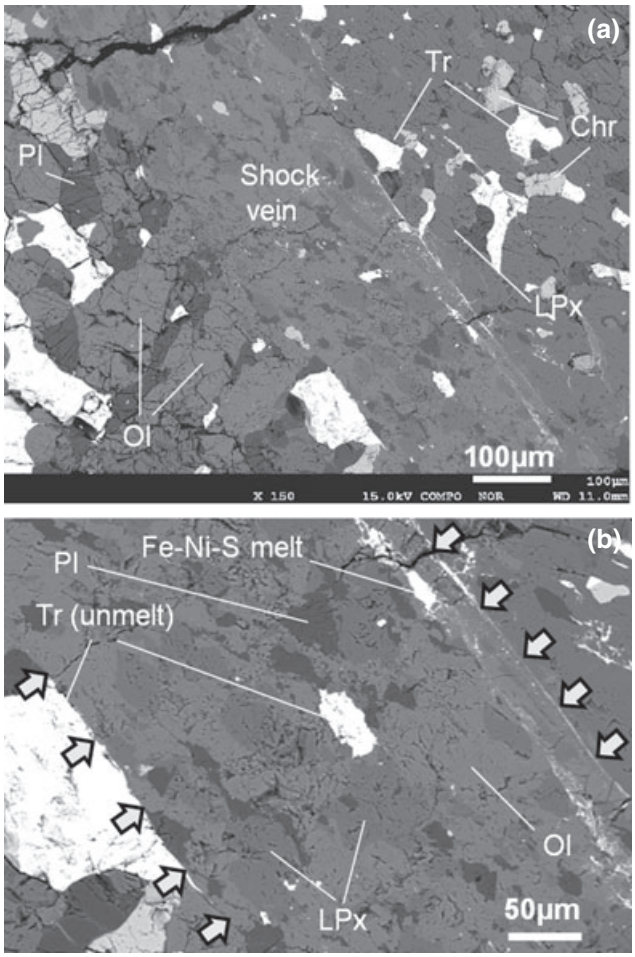

Fig. 9. BSE images of the Kilabo LL6 chondrite. a) A shock vein, going from upper left to lower right in the figure. b) An enlarged view of a lower right part of the shock vein (a), consisting mainly of olivine, low-Ca pyroxene, plagioclase, and troilite, with grain sizes smaller than those occurring in the typical LL6 lithology on either sides of the shock vein. Small amounts of Fe-Ni-S melt occur at the boundary to the host rock. Abbreviations: olivine (Ol), low-Ca pyroxene (LPx), plagioclase (Pl), chromite (Chr), and troilite (Tr).

by regolith migration and sorting toward the gravitational center of asteroid Itokawa (Miyamoto et al. 2007). Therefore, individual particles of MUSES-C Regio should have come from different locations and depths from the current Itokawa. Bulk composition of 50 Itokawa particles (Table 2) reveals depletion of troilite and FeNi metallic particles in MUSES-C Regio relative to LL chondrites, suggesting that mineral fractionation might have occurred during formation of MUSES-C Regio. On the other hand, even after the breakup and reaccretion of the asteroid and subsequent regolith migration, chemical compositions of silicate minerals at MUSES-C Regio retain a record of thermal metamorphism from the parent asteroid of Itokawa, unless the silicates were reheated at high temperature by subsequent impact events.

Olivine, low- and high-Ca pyroxene, plagioclase, and merrillite compositions are similar between the room A and the room B particles. This indicates that surface dust on the two touchdown sites of MUSES-C Regio has similar mineral chemistries. However, this conclusion must be carefully considered and verified, because the room A and B particles might have been mixed up either during the sample capture process on the asteroid and/or during up-and-down motions of the sample catcher in the course of curation work, as explained in the introduction. Recent investigation of many room B particles at JAXA showed that the abundance of plagioclase in room B seems to be higher than that in room A (Yada et al. 2012), implying that the room A and B particles were not well mixed.

Thermal Metamorphism of the Itokawa Parent Asteroid

Quantitative chemical compositions of silicates indicate that Itokawa dust particles have experienced thermal metamorphism, but not to a degree sufficient to thoroughly equilibrate them. Fa varies within individual particles and the degree of variation decreases in accordance with an increase of Fa (Fig. 5a). In addition, Fa and Fs of individual particles show a positive correlation (Fig. 5b). This trend suggests that olivine and pyroxene were heated within a single asteroid and most of them have neared final equilibration at around Fa = 30 and Fs = 24 during thermal metamorphism. Similar compositional trends were observed in LL3-5 ordinary chondrites (McCoy et al. 1991; Brearley and Jones 1998; Huss et al. 2006). It may be possible to explain the correlation of Fa and Fs (Fig. 5b) as a reduction of FeO in olivine and pyroxene during impact heating below melting temperature that occurred after thermal metamorphism. The in situ reduction of FeO would have produced small Fe metallic inclusions in the interior of olivine and pyroxene, but such inclusions have not been observed in these samples (Nakamura et al. 2011 and this study). Therefore, the compositional trend of olivine and low-Ca pyroxene (Fig. 5b) was not caused by impact heating in this case. Impact-induced compositional modification is limited only to compositional variations of plagioclase, as shown below.

Various mineral thermometers have been applied to Itokawa particles (Nakamura et al. 2011) and the results indicate that the peak temperature of thermal metamorphism was around 800 °C, as deduced from plagioclase triclinicity and two pyroxene thermometry. A simple onion-shell model for the thermal evolution of the Itokawa parent asteroid was developed (Wakita et al. 2013): the parent body should have been larger

than 20 km in radius and accreted between 1.9 and 2.2 Myr after CAI formation, to satisfy mineralogical and isotopic evidence (Nakamura et al. 2011; Yurimoto et al. 2011).

Compositional Modification During Cooling of the Itokawa Parent Asteroid

K-feldspar (sanidine) occurs in particle RA-QD02-0013 as exsolution lamellae in plagioclase (Fig. 6a and Nakamura et al. 2011). The quantitative chemical composition of a K-feldspar lamella with 2.5 μm width was obtained using a focused electron beam (<1 μm in diameter) of FE-EPMA, which permitted measurement of the composition of approximately 1×1 μm^2 area of K-feldspar without beam overlapping to coexisting plagioclase. The feldspar geothermometer (Fuhrman and Lindsley [1988] corrected by Kroll et al. [1993]) was applied to the plagioclase ($Ab_{85.0}An_{10.1}Or_{4.9}$) and the K-feldspar ($Ab_{13.9}An_{7.0}Or_{79.1}$), but a temperature of equilibration could not be obtained because the plagioclase and the K-feldspar were not an equilibrium pair at any temperature, probably due to compositional modification of the two minerals during cooling from the peak metamorphic temperature. Ab and Or contents are easier to change than An content, because diffusion rates of Na and K are faster than those of Ca in plagioclase, the latter involved a coupled substitution between CaAl and NaSi (Kasper 1975; Liu and Yund 1992; Cherniak 2010).

Kovach and Jones (2010) and Jones and Brearley (2011) found a similar exsolution texture in the Tuxtuac LL5 chondrite and applied feldspar geothermometry, but could not determine a temperature of equilibration. They set a priority on Ab content, which is more likely to be close to the equilibrium value than An content, and concluded that the measured compositions of exsolved pairs were more consistent with a low temperature, around 500 °C. When we plotted the compositions of our Itokawa data (particle RA-QD02-0013) on feldspar diagrams that show solvus and orientations of tie-lines of equilibrated compositional pairs for 500 and 757 °C (Kovach and Jones 2010), the Itokawa feldspars also show a closer match to solvus and tie-lines of 500 °C than those of 757 °C. This indicates that K-feldspar was likely to have exsolved from plagioclase at a peak temperature around 800 °C, which is deduced from plagioclase triclinicity (approximately 820 °C) and pyroxene thermometry (approximately 785 °C) for this particle (Nakamura et al. 2011). However, during slow cooling to 500 °C, Ab and Or contents of both plagioclase and K-feldspar were modified, but not the An content, resulting in an unequilibrated pair of plagioclase and K-feldspar.

Numerical Simulations for Ca Diffusion in Plagioclase During Cooling

We have performed numerical simulations to understand the compositional changes of feldspar during cooling of the Itokawa parent asteroid. We assume that the parent asteroid measured 50 km in diameter and formed 2.2 Myr after CAIs (Wakita et al. 2013). Because with these conditions the Itokawa parent asteroid reaches a peak temperature very close to 800 °C, we calculated the diffusion length of Ca in plagioclase at the center of the asteroid during cooling from 800 to 500 °C (Fig. 10). Because plagioclase is coarser than K-feldspar and Ca diffusion is slower than Na and K diffusion (Cherniak 2010), Ca in plagioclase is most difficult to homogenize during cooling. We adopted two different CaAl-NaSi interdiffusion rates to our calculations, because the diffusion rates are known to increase with increasing pressures and water contents (Cherniak 2010). The higher rate we used was experimentally determined under conditions of high pressure (1500 MPa) and hydrous conditions (approximately 1 wt% water) (Liu and Yund 1992). On the other hand, the lower rate we used is obtained in dry and low-pressure (1 atm.) conditions, but the ratio is only given as an upper bound ($D < 10^{-21}$ m^2 s^{-1} at 1100 °C: Yund 1986). Thus, the results of our Ca diffusion calculation for dry conditions (Fig. 10) also give an upper limit and the actual length may have been smaller.

The results of the calculation (Fig. 10) indicate that it took 4.4 Myr to cool from 800 to 500 °C in a 50 km sized body and Ca diffusion lengths are 42 and 4 μm for wet and high-pressure conditions and for dry and low-pressure conditions, respectively. The diffusion was almost complete at around 700 °C and below this temperature the diffusion length did not increase (Fig. 10). On the other hand, the size of plagioclase in Itokawa particles ranges from 20 to 50 μm (Nakamura et al. 2011). Therefore, if the Itokawa parent asteroid contained a low abundance of water, then the An content of plagioclase would not have equilibrated during cooling and thus records high-temperature compositions, as found in plagioclase in RA-QD02-0013. On the contrary, Na-K interdiffusion is at least several orders of magnitude faster that NaSi-CaAl interdiffusion, which reflects the relatively rapid exchange of univalent alkali cations (Cherniak 2010). Therefore, during cooling of a 50 km sized body (Fig. 10), Ab and Or contents were easily equilibrated in 20 to 50 μm sized plagioclase. This indicates that Ab content records the lower equilibrium temperature (approximately 500 °C in the case of RA-QD02-0013), confirming the interpretation by Kovach and Jones (2010).

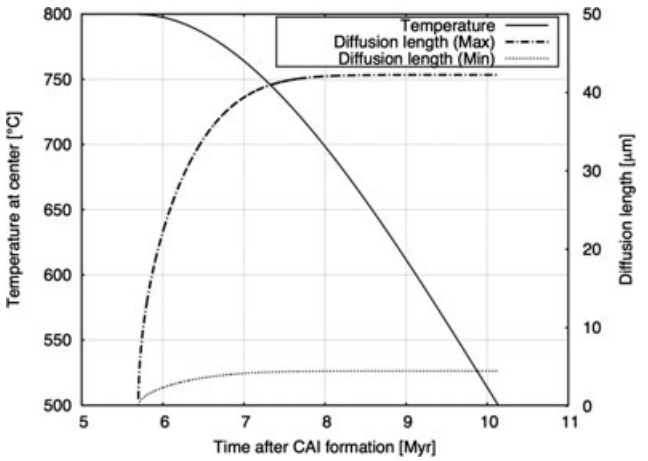

Fig. 10. Temperature and Ca diffusion lengths in plagioclase crystals at the center of the Itokawa parent asteroid as a function of time after CAI formation. The asteroid formed 2.2 Myr after CAIs as a body 25 km in radius. Pressure at the center is approximately 1MPa assuming 3.4 g cm^{-3} density that is calculated from relative mineral abundance in Itokawa particles (Tsuchiyama et al. 2011). The heat source of the asteroid is the decay energy of ^{26}Al and $(^{26}Al/^{27}Al)_0$ at the time of CAI formation is assumed to be 5×10^{-5}. The center of the asteroid reaches a peak temperature of 800 °C and the temperature decreases from 800 °C (at 5.7 Myr after CAIs) to 500 °C (at 10.1 Myr after CAIs). During cooling, cation redistribution takes place between plagioclase and K-feldspar. We calculate Ca diffusion lengths in plagioclase in two extreme cases. CaAl-NaSi interdiffusion rates at each temperature are calculated from activation energies and pre-exponential factors from the literature. "Diffusion length (Max)" in the figure is a result obtained using a highest diffusion rate (CaAl-NaSi interdiffusion of albitic plagioclase (An0-26) under 1500MPa and hydrous conditions: Liu and Yund 1992). 1500 MPa corresponds to the pressure of the center of a 2000 km sized body like the Moon, which is much larger than 50 km Itokawa parent asteroid. On the other hand, an activation energy and a pre-exponential factor for CaAl-NaSi interdiffusion in albitic plagioclase under low-pressure and dry conditions have not yet been fully determined (Cherniak 2010). Therefore, for the calculation of "Diffusion length (Min)" in the figure, we assume the activation energy is the same as that for hydrous and high-pressure conditions (303 kJ mol^{-1}: Liu and Yund 1992) and calculate a pre-exponential factor from the upper bound of a CaAl-NaSi interdiffusion rate in albitic plagioclase (An0-26) at 0.1MPa and 1100 °C under dry conditions ($D < 10^{-21}$ m^2 s^{-1}: Yund 1986). The actual activation energy may have been higher than 303 kJ mol^{-1} because, in the case of anorthite, the activation energy is higher under hydrous conditions than under dry conditions. Therefore, the "Diffusion length (Min)" in the figure gives the upper bound for Ca diffusion under the low-pressure and dry conditions.

Impact-Induced Disturbance of Na-K Distribution in Plagioclase

Many MUSES-C particles experienced impacts after thermal metamorphism, with the largest impact destroying the parent asteroid of Itokawa. In this section, we focus on shock-induced disturbance of the plagioclase Na-K distribution, because shock heating effects on chemical composition are clearly seen in plagioclase, but not evident in olivine and pyroxene, as is observed in the Kilabo meteorite (Table 3). Plagioclase in MUSES-C particles shows a large Ab-Or variation (Fig. 7a), but the variation resulted from wide variations of some particular particles. For instance, plagioclase in RA-QD02-0051 ($Ab_{82.6 \pm 2.3}An_{11.2 \pm 0.7}Or_{6.2 \pm 2.2}$) and RA-QD02-0031 ($Ab_{83.0 \pm 2.3}An_{10.4 \pm 1.0}Or_{6.6 \pm 1.7}$) shows Ab-Or variations much larger than those in RA-QD02-0061 ($Ab_{84.7 \pm 0.7}An_{11.3 \pm 0.5}Or_{4.0 \pm 0.3}$) and RA-QD02-0058 ($Ab_{86.4 \pm 0.9}An_{10.4 \pm 0.9}Or_{3.1 \pm 0.3}$). The large Ab-Or variations of the former two particles are ascribed to impact-induced heating that occurred *after* cooling from a long-duration thermal metamorphism, while the small Ab-Or variations in the latter two particles were established *during* cooling from a peak metamorphic temperature. This interpretation is supported by the observation of the Kilabo meteorite, because the same compositional differences are observed between a shock vein and adjacent host rock (Figs. 9a and 9b). Plagioclase in the shock vein shows a wide Ab-Or variation toward a Na-poor component, while that in the typical LL6 lithology is Na-rich and shows small Ab-Or variations (Fig. 7c; Table 3). This clearly indicates that impact heating caused disturbance of the Na-K distribution in plagioclase, most likely due to partial Na evaporation induced by heterogeneous temperature distribution within the shock vein.

Our results from analyses of individual Itokawa particles reveal that they underwent thermal metamorphism, slow cooling from a peak metamorphic temperature, and postmetamorphism impacts heating, as were also recorded in many ordinary chondrites (Rubin 2004).

SUMMARY

The mineralogy and mineral chemistry of 48 Itokawa dust particles were characterized. The particles collected at the first touchdown show mineral chemistries similar to those collected at the second touchdown. Most particles suffered thermal metamorphism in the asteroid, but are not completely equilibrated. Slow cooling from a peak temperature modified plagioclase and K-feldspar composition. Some of the particles seem to have experienced postmetamorphic reheating resulting from impacts, which resulted in modification of the Na-K distribution in plagioclase.

Acknowledgments—We thank the Hayabusa project team for the sample return; KEK and SPring-8 for

synchrotron experiments; the Global COE project at Tohoku University for financial support; Drs. Hokada and Ikeda for discussion; Drs. Nakao, Yamazaki, Shimada, Kakazu, Tazawa, Matsuoka, Matumoto, Matsuno, Katsuya, Matsushita, Sugimoto, and Aoki for technical support; and Drs. Ruzicka, Jones, and Ogliore for constructive reviews of the manuscript. Tomoki Nakamura is supported by a grant from Ministry of Education, Technology, and Science (No. 21340165). Michael Zolensky and Scott Sandford acknowledge the NASA Muses-CN Program for support.

Editorial Handling—Dr. Alex Ruzicka

REFERENCES

Abe M., Takagi Y., Kitazato K., Abe S., Hiroi T., Vilas F., Clark B. E., Abell P. A., Lederer S. M., Jarvis K. S., Nimura T., Ueda Y., and Fujiwara A. 2006. Near-infrared spectral results of asteroid Itokawa from the Hayabusa spacecraft. *Science* 312:1334–1338.

Binzel R. P., Rivikin A., Bus S., Sunshine J., and Burbine T. 2001. MUSES-C target asteroid (25143) 1998 SF36: A reddened ordinary chondrite. *Meteoritics & Planetary Science* 36:1167–1172.

Brearley A. J. and Jones R. H. 1998. Chondritic meteorites. In *Planetary materials*, edited by Papike J. J. Reviews in Mineralogy, vol. 36. Washington, D.C.: Mineralogical Society of America. pp. 3-1–3-398.

Chen M. and El Goresy A. 2000. The nature of maskelynite in shocked meteorites: Not diaplestic glass but a glass quenched from shocked-induced dense melt at high pressures. *Earth and Planetary Science Letters* 179:489–502.

Cherniak D. J. 2010. Cation diffusion in feldspars. In *Diffusion in minerals and melts*, edited by Zhang Y. and Cherniak D. J. Reviews in Mineralogy and Geochemistry, vol. 72. Washington, D.C.: Mineralogical Society of America. pp. 691–733.

Dunn T. L., Cressey G., McSween H. Y. Jr., and McCoy T. J. 2010. Analysis of ordinary chondrites using powder X-ray diffraction: 1. Modal mineral abundances. *Meteoritics & Planetary Science* 45:123–134.

Ebihara M., Sekimoto S., Shirai N., Hamajima Y., Yamamoto M., Kumagai K., Oura Y., Ireland T. R., Kitajima F., Nagao K., Nakamura T., Naraoka H., Noguchi T., Okazaki R., Tsuchiyama A., Uesugi M., Yurimoto H., Zolensky M. E., Abe M., Fujimura A., Mukai T., and Yada T. 2011. Neutron activation analysis of a particle returned from asteroid Itokawa. *Science* 333:1119–1121.

Ebihara M., Shirai N., Sekimoto S., Nakamura T., Tsuchiyama A., Matsuno J., Matsumoto T., Abe M., Fujimura A., Mukai T., Uesugi M., and Yada T. Forthcoming. Chemical composition of tiny grains recovered from an asteroid Itokawa: An INAA study. *Meteoritics & Planetary Science*.

Fuhrman M. L. and Lindsley D. H. 1988. Ternary feldspar modeling and thermometry. *American Mineralogist* 73:201–215.

Huss G. R., Rubin A. E., and Grossman J. N. 2006. Thermal metamorphism in chondrites. In *Meteorites and the early solar system II*, edited by Lauretta D. S. and McSween H. Y. Jr. Tucson, Arizona: The University of Arizona Press. pp. 567–586.

Jarosewich E. 1990. Chemical analysis of meteorites: A compilation of stony and iron meteorite analysis. *Meteoritics* 25:323–337.

Jones R. H. 1997. Equilibration of pyroxenes in type 4-6 LL chondrites (abstract #1217). 28th Lunar and Planetary Science Conference. CD-ROM.

Jones R. H. and Brearley A. J. 2011. Exsolution in feldspar in the Tuxtuac (LL5) chondrite: A new perspective on cooling rates for metamorphosed chondrites. 74th Annual Meteoritical Society Meeting (abstract #5475).

Kasper R. B. 1975. Cation and oxygen diffusion in albite. Ph.D. thesis, Brown University, Providence, Rhode Island.

Kawaguchi J., Aida S., and Morita H. 2006. Hayabusa, Detailed guidance and navigation operations during descents and touchdowns. AIAA/AAS Astrodynamics Specialist Conference and Exhibit. AIAA 2006-6536:1–16.

Kovach H. A. and Jones R. H. 2010. Feldspar in type 4-6 ordinary chondrites: Metamorphic processing on the H and LL chondrite parent bodies. *Meteoritics & Planetary Science* 45:246–264.

Kroll H., Evangelakakis C., and Vall G. 1993. Two-feldspar geothermometry: A review and revision for slowly cooled rocks. *Contributions to Mineralogy and Petrology* 114:510–518.

Lindsley D. H. 1983. Pyroxene geothermometry. *American Mineralogist* 68:477–493.

Liu M. and Yund R. A. 1992. NaSi-CaAl interdiffusion in plagioclase. *American Mineralogist* 77:275–283.

McCoy T. J., Scott E. R. D., Jones R. H., Keil K., and Taylor G. J. 1991. Composition of chondrule silicates in LL3-5 chondrites and implications for their nebular history and parent body metamorphism. *Geochimica et Cosmochimica Acta* 55:601–619.

McSween H. Y. and Patchen A. D. 1989. Pyroxene thermobarometry in LL-group chondrites and implications for parent body metamorphism. *Meteoritics* 24:219–226.

Miyamoto H., Yano H., Scheeres D. J., Abe S., Barnouin-Jha O., Cheng A. F., Demura H., Gaskell R. W., Hirata N., Ishiguro M., Michikami T., Nakamura A. M., Nakamura R., Saito J., and Sasaki S. 2007. Regolith migration and sorting on asteroid Itokawa. *Science* 316:1011–1014.

Nagao K., Okazaki R., Nakamura T., Miura Y. N., Osawa T., Bajo K., Matsuda S., Ebihara M., Ireland T. R., Kitajima F., Naraoka H., Noguchi T., Tsuchiyama A., Uesugi M., Yurimoto H., Zolensky M., Shirai K., Abe M., Yada T., Ishibashi Y., Fujimura A., Mukai T., Ueno M., Okada T., Yoshikawa M., and Kawaguchi J. 2011. Irradiation history of Itokawa regolith material deduced from noble gases in the Hayabusa samples. *Science* 333:1128–1131.

Nakamura T., Noguchi T., Tanaka M., Zolensky M. E., Kimura M., Tsuchiyama A., Nakato A., Ogami T., Ishida H., Uesugi M., Yada T., Shirai S., Fujimura A., Okazaki R., Sandford S. A., Ishibashi Y., Abe M., Okada T., Ueno M., Mukai T., Yoshikawa M., and Kawaguchi J. 2011. Itokawa dust particles: A direct link between S-type asteroids and ordinary chondrites. *Science* 333:1113–1116.

Nittler L. R., Starr R. D., Lev L., McCoy T. J., Burbine T. H., Reedy R. C., Trombka J. I., Gorenstein P., Squyres S. W., Boynton W. V., Mcclanahan T. P., Bhangoo J. S., Clark P. E., Murphy M. E., and Killen R. 2001. X-ray

fluorescence measurements of the surface elemental composition of asteroid 433 Eros. *Meteoritics and Planetary Science* 36:1673–1695.

Noguchi T., Nakamura T., Kimura M., Zolensky M. E., Tanaka M., Hashimoto T., Konno M., Nakato A., Ogami T., Fujimura A., Abe M., Yada T., Mukai T., Ueno M., Okada T., Shirai K., Ishibashi Y., and Okazaki R. 2011. Incipient space weathering observed on the surface of Itokawa dust particles. *Science* 333:1121–1125.

Rubin A. E. 1992. A shock-metamorphic model for silicate darkening and compositionally variable plagioclase in CK and ordinary chondrites. *Geochimica et Cosmochimica Acta* 56:1705–1714.

Rubin A. E. 2004. Postshock annealing and postannealing shock in equilibrated ordinary chondrites: Implications for the thermal and shock histories of chondritic asteroids. *Geochimica et Cosmochimica Acta* 68:673–689.

Russell S. S., Zipfel J., Folco L., Jones R., Grady M. M., McCoy T., and Grossman J. N. 2003. The Meteoritical Bulletin, No. 87, 2003 July. *Meteoritics & Planetary Science* 87:189–248.

Stöffler D., Keil K., and Scott E. R. D. 1991. Shock metamorphism of ordinary chondrites. *Geochimica et Cosmochimica Acta* 55:3845–3867.

Tanaka M., Nakamura T., Noguchi T., Nakato A., Ishida H., Yada T., Shirai K., Fujimura A., Ishibashi Y., Abe M., Okada T., Ueno M., and Mukai T. 2013. Crystallization temperature determination of Itokawa particles by plagioclase thermometry with X-ray diffraction data obtained by a high-resolution synchrotron Gandolfi camera. *Meteoritics & Planetary Science*, doi:10.1111/maps.12215.

Tsuchiyama A., Uesugi M., Matsushima T., Michikami T., Kadono T., Nakamura T., Uesugi K., Nakano T., Sandford S. A., Noguchi R., Matsumoto T., Matsuno J., Nagano T., Imai Y., Takeuchi A., Suzuki Y., Ogami T., Katagiri J., Ebihara M., Ireland T. R., Kitajima F., Nagao K., Naraoka H., Noguchi T., Okazaki R., Yurimoto H., Zolensky M. E., Mukai T., Abe M., Yada T., Fujimura A., Yoshikawa M., and Kawaguchi J. 2011. Three-dimensional structure of Hayabusa samples: Origin and evolution of Itokawa regolith. *Science* 333:1121–1125.

Tsuchiyama A., Uesugi M., Uesugi K., Nakano T., Noguchi R., Matsumoto T., Matsuno J., Nagano T., Imai Y., Shimada A., Takeuchi A., Suzuki Y., Nakamura T., Noguchi T., Abe M., Yada T., and Fujimura A. 2013. Three-dimensional microstructure of samples recovered from asteroid 25143 Itokawa: Comparison with LL5 and LL6 chondrite particles. *Meteoritics & Planetary Science*, doi:10.1111/maps.12177.

Van Schmus W. R. and Wood J. A. 1967. A chemical-petrologic classification for the chondritic meteorites. *Geochimica et Cosmochimica Acta* 31:747–765.

Wakita S., Nakamura T., Ikeda T., and Yurimoto H. 2013. Thermal modeling for a parent body of Itokawa. *Meteoritics & Planetary Science*, doi:10.1111/maps.12174.

Yada T., Abe M., Okada T., Uesugi M., Karouji Y., Ishibashi Y., Yakame S., Shirai K., Nakamura T., Noguchi T., Okazaki R., and Fujimura A. 2012. Mineral ratios of Itokawa particles recovered from the Hayabusa sample catcher (abstract #5245). 75th Annual Meeting of the Meteoritical Society. *Meteoritics & Planetary Science* 47.

Yano H., Kubota T., Miyamoto H., Okada T., Scheeres D., Takagi Y., Yoshida K., Abe M., Abe S., Barnouin-Jha O., Fujiwara A., Hasegawa S., Hashimoto T., Ishiguro M., Kato M., Kawaguchi J., Mukai T., Saito J., Sasaki S., and Yoshikawa M. 2006. Touchdown of the Hayabusa spacecraft at the Muses Sea on Itokawa. *Science* 312:1350–1353.

Yund R. A. 1986. Interdiffusion of NaSi-CaAl in peristerite. *Physics and Chemistry of Minerals* 13:11–16.

Yurimoto H., Abe K., Abe M., Ebihara M., Fujimura A., Hashiguchi M., Hashizume K., Ireland T. R., Itoh S., Katayama J., Kato C., Kawaguchi J., Kawasaki N., Kitajima F., Kobayashi S., Meike T., Mukai T., Nagao K., Nakamura T., Naraoka H., Noguchi T., Okazaki R., Park C., Sakamoto N., Seto Y., Takei M., Tsuchiyama A., Uesugi M., Wakaki S., Yada T., Yamamoto K., Yoshikawa M., and Zolensky M. E. 2011. Oxygen isotopic compositions of asteroidal materials returned from Itokawa by the Hayabusa mission. *Science* 333:1116–1119.